On the use of instrumented indentation to characterize the mechanical properties of functionally graded binary alloys manufactured by additive manufacturing

Catherine Schneider-Maunoury, Alaa Albayda, Olivier Bartier, Laurent Weiss, Gerard Mauvoisin, Xavier Hernot, Pascal Laheurte

On the use of instrumented indentation to characterize the mechanical properties of functionally graded binary alloys manufactured by additive manufacturing

C. SCHNEIDER-MAUNOURY[1], A. ALBAYADA[2], O. BARTIER[2], L. WEISS[1,], G. MAUVOISIN[2], X. HERNOT[2], P. LAHEURTE[1]

[1]Université de Lorraine, CNRS, Arts et Métiers ParisTech, LEM3, F-57000, Metz, France

[2]LGCGM, Université Rennes 1, 3 Rue du Clos Courtel 35700 Rennes, France

**Corresponding author: olivier.bartier@univ-rennes1.fr*

Abstract

The mechanical properties of a Ti-xNb functionally graded material (FGM) created by using an additive manufacturing process (CLAD®) were obtained using a spherical instrumented indentation test (IIT). The aim of this paper is to demonstrate the great suitability of the indentation test coupled with FGM for not only obtaining the hardness of a material, but also obtaining other mechanical properties such as Young's modulus, yield stress and the work-hardening exponent for heterogeneous materials. In the first step, results obtained from the instrumented indentation test were compared with those obtained from the tensile test for the same materials. These results show that these two tests highlight a similar evolution in the mechanical properties. In the second step, and after validating the efficiency of the IIT in obtaining mechanical properties, the FGM Ti-xNb was successfully identified using only IIT. This paper demonstrates that the different mechanical properties of all the compositions of a phase diagram can be measured very easily and quickly while minimizing the number of samples.

Keywords: Functionally graded material, Titanium-niobium alloys, Additive manufacturing, Instrumented indentation test, Tensile test

1. Introduction

Additive manufacturing, also known as 3D printing, is a process that creates a physical object from a digital design. Developed in the 1980s, additive manufacturing is undergoing rapid growth as it is spreading its contribution to different fields and sectors such as biomedical design, aerospace and automotive engineering [1]. Additive manufacturing is mainly divided into two groups: Powder Bed Fusion (PBF) and Direct Energy Deposition (DED). These processes are defined in ASTM F2792 [2] and are used for distinct applications due to their specific properties (part size, microstructures, scanning speed…). Regardless of the process, parts are obtained layer by layer to attain the desired geometry. Moreover, these processes can both be used to obtain more complex materials such as a Functionally Graded Materials (FGM). For example, Chlebus et al. manufactured Ti-xRe alloys with the PBF process [3], Collins et al. used the DED-LENS™ process to manufacture Ti-xV alloys [4] and Carroll et al. realized functionally graded 304L-IN625 alloys by DED process [5] .

FGMs are materials that have different mechanical properties within their volume, and that therefore can exhibit special functionalities. They have been commonly applied in engineering sciences in the last thirty years [6]–[11]. Contrary to PBF processes, CLAD®, which is a derivative of DED processes, consists in injecting powders in a laser beam, leading to easier manufacturing of FGMs parts. As the development of FGMs rapidly increases, the accuracy in determining their mechanical properties becomes a main point of focus [5], [12]. Therefore, an extensive understanding of their mechanical behaviours allows designing and achieving advanced functionalities.

Uniaxial tests such as tensile, compression or shear testing provide a simple and effective means of characterizing the materials' response to loading. These mechanical tests require preparation of specimens with a standardized cross section. For example, the tensile test specimens must have two shoulders and a gauge (section). They are placed in a testing machine and may be slowly extended until fracture (during the tensile tests) or buckling (during the compression tests). In the case of a FGM divided into many layers, uniaxial loading tests only characterize the general behaviour of the whole material rather than the behaviour of each layer of the tested specimen. Thus, in order to identify each part of the complex material, a localized testing is recommended.

One of the most used local tests is the instrumented indentation test (IIT) derived from hardness tests which are widely used in mechanical engineering. The original tests consist in determining the normalized Vickers, Brinell and Rockwell hardness. After decades of theoretical developments, the indentation test now enables the determination of other mechanical properties such as Young's modulus, the yield strength and the work-hardening exponent [13]–[19]. Its applications in mechanical characterization has been demonstrated in many papers [16], [20]–[27]. In most of these papers, a Hollomon's power law describes the plastic hardening, whereas the elastic portion follows Hooke's law. The continuity of the stress-strain curve at the elastic limit results in:

$$\sigma = E\varepsilon \quad \text{(Hooke)} \qquad \text{if } \varepsilon \leq \sigma_y/E \tag{1}$$

$$\sigma = E^n \sigma_y^{(1-n)} \varepsilon^n \quad \text{(Hollomon)} \qquad \text{if } \varepsilon > \sigma_y/E$$

where E is Young's Modulus, σ_y is the yield stress and n is the strain hardening exponent.

In the present paper, a FGM Ti-xNb alloy (where x=0, 26, 48, 75 and 100 wt%) obtained by additive manufacturing is characterized using the instrumented indentation test (IIT). Previously, in order to validate the results obtained by the IIT, different tensile specimens for homogeneous Ti-xNb materials with x=5, 10, 40 and 70 wt% were manufactured by the same process and then tested using both tensile and indentation tests.

Thus, the aim of this paper is to demonstrate the potential use of instrumented indentation to characterize the evolution of the mechanical properties of heterogeneous materials such as FGMs. This is especially useful when it is very difficult to machine viable tensile test specimens as it is the case with the Ti64-Mo alloy obtains by additive manufacturing [28]. Before proceeding to the experimental characterization, an explanation of instrumented indentation principle is presented.

2. Instrumented indentation principle

An instrumented indentation test (IIT) consists in inserting an indenter tip, whose geometry is known, into a specific location of the tested material by applying an increasing normal load (F) or a known displacement (h). This penetration results in a load-displacement curve called F(h) (fig.1). The curve F(h) that is acquired from the material penetration test enables the quantification of the mechanical properties of the tested material.

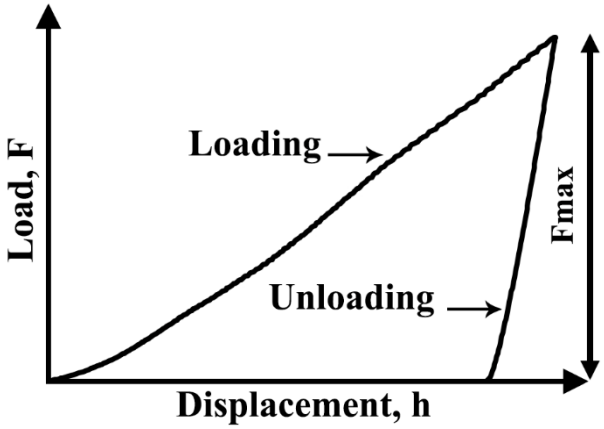

Figure 1: Indentation load-displacement curve

2.1 Determination of the hardness

In 1951, Meyer [29] proposed the following equation in order to determine the hardness of the material:

$$H = \frac{F}{\pi a^2} \tag{2}$$

where H is the contact pressure (hardness), F is the maximum concentrated load applied on the sample, and "a" is the contact radius between the indenter and the sample. In practice, "a" can be determined from an optical microscopic image of the imprint after each indentation test or can be deduced from the indentation curve [18].

2.2 Determination of the elastic properties

The Young's Modulus of a material is determined from the unloading part of the F(h) curve since the removal depends on the elastic return caused by the elasticity of the material.

From the material's contact rigidity, the reduced elastic modulus can be calculated according to BASh formula (eq.3) [30], [31]:

$$E_R = \frac{\sqrt{\pi}\, S}{2\sqrt{A}} \tag{3}$$

where E_R is the reduced elastic modulus, A is the contact area between the indenter and the sample, and S is the contact stiffness.

Taking into account the elasticity of the material as well as that of the indenter, the reduced elastic modulus of the material is defined by eq.4:

$$\frac{1}{E_r} = \frac{1-\nu^2}{E} + \frac{1-\nu_i^2}{E_i} \quad (4)$$

where E_i and ν_i are the elastic modulus and the Poisson's coefficient of the indenter respectively, E and ν are the elastic modulus and the Poisson's coefficient of the studied material respectively.

The BASh's formula does not take into account radial displacements caused by the vertical pressure, which are significant for deep indentations. In 2001, Hay and Wolff [32] proposed a correction factor that could take into account these radial displacements in the case of spherical contact. Thus, eq.3 becomes:

$$E_r = \frac{S}{2\gamma a} \quad (5)$$

where γ is the correction factor proposed by Hay and Wolff [32].

The value of γ depends on the contact radius "a" and the contact elastic parameters. It is calculated by iterative method that leads to γ values slightly greater than 1. In consequence, the use of eq.5 results in E_R values lower than those obtained with eq.3.

2.3 Determination of the work-hardening law

The work-hardening law is determined from the loading part of the indentation curve (fig.1). Assuming that the material is isotropic and the hardening law is also isotropic following Hollomon's power law given in eq.1, with two parameters to be identified (σ_y and n), the method of identification of Moussa et al. is used [17].

This method consists in calculating the error between an experimental F(h) curve and a number of F(h) curves obtained from a finite element (FE) simulation. In order to quantify the difference between the experimental and numerical indentation curves, the root mean square error defined by eq.6 was used:

$$E_{RMS}(h_{max}/R) = \sqrt{\frac{1}{h_{max}}\int_0^{h_{max}} \left(F_{exp} - F_{num}\right)^2 dh} \quad (6)$$

where R is the spherical indenter radius, h_{max} is the maximal penetration depth and F_{exp} and F_{num} are the load from both experimental and numerical curves, respectively. To use this method, a database of FE simulation indentation curves was built up with 3872 F(h) curves. The corresponding Hollomon's hardening law parameter sets (σ_y, n) were presented in a previous paper [17]. The characterization procedure leads to the determination of the hardening law for homogenous materials using the average representative strain concept. Contrary to the other methods [13], [15], [23], the method of identification of Moussa et al. is not based on an empirical formula and is able to calculate the representative strain directly from the response of the indentation test. Using different penetration depths provides the range of strain for which the identified hardening law is the most precise. For spherical indentation, the range of the representative strain values is equal to about 0.013-0.045 for Cao and Lu [13], 0.04-0.07 for Zhao et al. [19] and 0.01-0.06 for Moussa et al. [17], depending on the *h/R* values. This method gives not only an optimal solution, but also a solution domain and a confidence interval that takes into account not only the material's heterogeneity but also experimental imprecisions.

3. Materials and experimental procedure

3.1 Powder characteristics

The materials used for the Ti-xNb alloy are pure titanium powder provided by TLS Technik and pure niobium provided by H.C. Starck Tantalum and Niobium GmbH. The pure titanium powder had a particle size distribution of between 45 and 90 µm (D50 = 73 µm). Due to the gap between the melting points of the two powders (Tf_Nb = 2467 °C and Tf_Ti = 1670 °C) [33], the particle size distribution of pure niobium is below 63 µm in order to facilitate the melting of these powders (D50 = 56 µm).

All the powders are spherical with some satellites, and were deposited onto a Ti6Al4V substrate (100 mm * 100 mm * 8 mm).

3.2 CLAD® process

The powders were deposited by using CLAD®, an additive manufacturing process which alloys different powders together and manufactures 3D parts. The equipment required for this process consists of a coaxial nozzle that had been adapted to manufacture refractory materials such as niobium or molybdenum. A 2 kW laser diode characterized by a 980 nm wavelength, a 600 µm fibre diameter and a focal distance at 12.5 mm was also part of the equipment. As this experiment involved titanium, a metal that reacts with oxygen, the manufacturing was mostly carried out under argon gas. Thus, the oxygen concentration was maintained below 20 ppm and that of H_2O was kept below 50 ppm.

To control the *in situ* variation of the chemical composition of the powders in order to successfully manufacture functionally graded parts, a differential injection was used. This system allows the homogenisation of the mixed powders and the control of the gas flow. The dry mix was then injected into the nozzle before being deposited onto the substrate (fig.2).

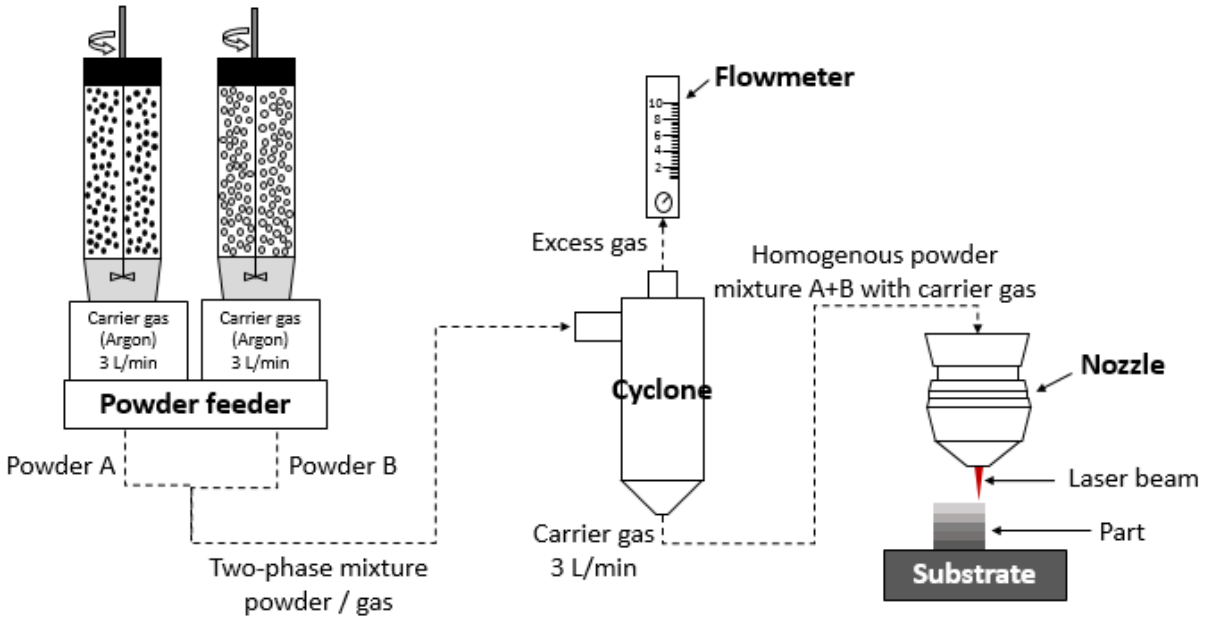

Figure 2: Differential injection principle

The process parameters were adjusted according to the chemical composition of each zone of the FGM: 1500-2000 W for laser power, 1500-2000 mm/min for travel speed, 0-20 g/min for powder feed rate and 0-0.8 mm for layer height step [28], [34].

The part manufactured in this work was composed of 5 layers of different chemical composition, as shown in fig.3 with the example of a Ti-xNb alloy (where x = 0, 26, 48, 75 and 100 wt%).

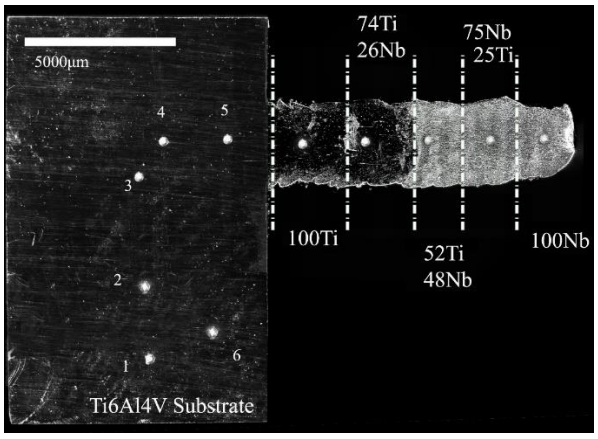

Figure 3: Chemical composition of each zone of the Ti-Nb wall, and position of indentation in the wall and in the substrate realized in face 1 of the Ti-Nb part

3.3 Tensile test

In order to characterize the different Ti-xNb chemical compositions, four homogeneous walls were made by additive manufacturing with the following Nb wt%: 5%, 10%, 40% and 70%.

For each composition, 4 tensile specimens of rectangular cross-section were taken in the build direction. The flat specimens have a cross-section of 8x2 mm^2 and a gauge length of 40 mm. To avoid any microstructure modification during the preparation, the walls were first carefully milled and then bone-shaped uniaxial tensile specimens were cut using a water jet process. The mechanical properties were examined from conventional tensile tests until rupture. This was carried out on a Zwick 100 kN machine with a strain rate of $10^{-4}\,s^{-1}$ and the data were processed with Test Xpert II. An extensometer was used to precisely measure the deformation of the specimens.

3.4 Instrumented indentation

Indentation tests were carried out using an instrumented indentation setup developed in the LGCGM laboratory. This testing system can apply high indentation loads unlike most commercially available setup. For high loading levels, precise determination of the setup compliance is a necessity. The originality of our experimental bench is that it allows the direct measurement of the distance between the tested surface and the tip of the indenter, which avoids calculating the conformity of the machine

The indenter used is almost spherical with a radius of 0.25 mm made of tungsten carbide. The Young's modulus and the Poisson's ratio were equal to 600 GPa and 0.23, respectively. The indentation load was obtained with a resolution of 0.02 N from a load cell located below the sample and the displacement was measured thanks to capacitive sensors. Three capacitive sensors were used to measure the distance between the indenter and the indented surface of the tested material with a resolution of 0.02 µm. These sensors were fixed near the indenter tip.

In order to characterize the functionally graded wall, it is necessary to first validate the characterization of the Ti-Nb alloy by using instrumented indentation and tensile tests.

4. Validation of the methodology based on the Instrumented Indentation Test

An Instrumented Indentation Test (IIT), as explained previously, is a local test by which mechanical properties such as Young's modulus or the hardening law can be obtained. The aim of this paragraph is to validate this method by studying the influence of the geometry of the tested sample on the mechanical properties, and comparing the results with another characterization test: the tensile test.

4.1 Numerical investigation on the Ti-Nb alloy

The numerical investigation was performed in order to verify the influence of the dimension of the thin wall shown in fig.3 on the determination of the mechanical properties via IIT. In other words, the influence of Boundary Conditions (BC) on F(h) curves obtained from spherical indentation tests is studied.

For this investigation, a pseudo-material following Hollomon's law is considered and the elasto-plastic behaviour with Von-Mises criterion was chosen with E=113.8 GPa, σ_y=880 MPa, ν=0.34 and n=0.0716 referring

to a Ti6Al4V solution-treated and aged alloy [35]. The behaviour of the spherical indenter with R=0.25 mm was considered elastic with E_{ind}=600 GPa, ν_{ind}=0.23 and R=0.25 mm.

To simulate the indentation test, the FE (Finite Element) software "Abaqus" was used. Simulations were undertaken using two different types of mesh: a 2D axisymmetric mesh referring to an infinite half-space (2D s984 mesh given in fig.4) and a 3D mesh model that represents the thin wall of the real tested Ti-Nb specimen (3D th3H7 mesh given in fig.5). Four-nodded axisymmetric elements (CAX4) and eight-node brick elements (C3D8) were used for both, 2D and 3D models, respectively. Large displacements and deformation options were chosen in Abaqus. The sliding was considered finite which allowed for arbitrary sliding and rotation of contact surfaces as it also included effects due to he non-geometrical linearity. The contact was established with a penalty algorithm and was characterized by a Coulomb friction coefficient of 0.1.

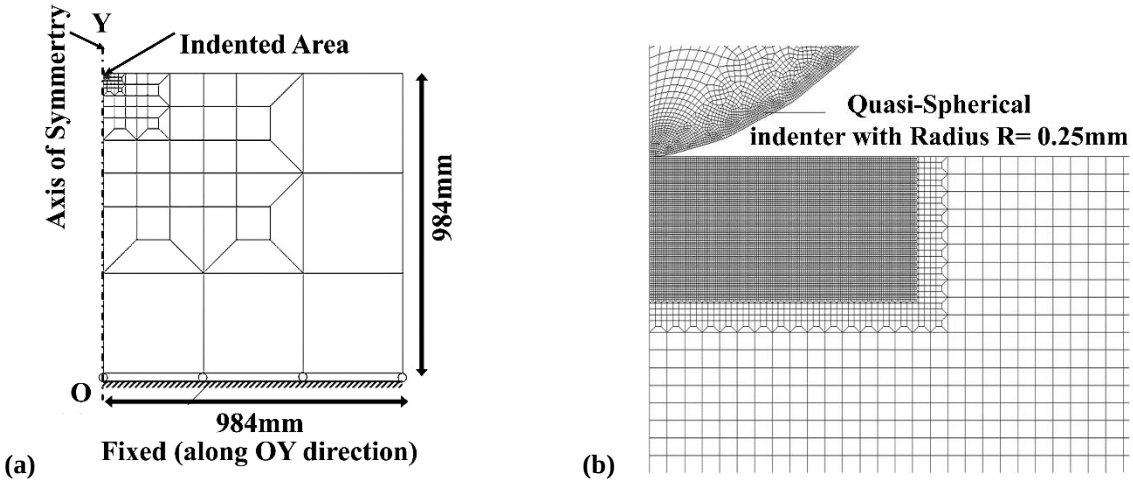

Figure 4: 2D Mesh (2D s984) corresponding to a 984 mm side square sample (a) complete mesh with BC and (b) zoom near the 0.25 mm indenter

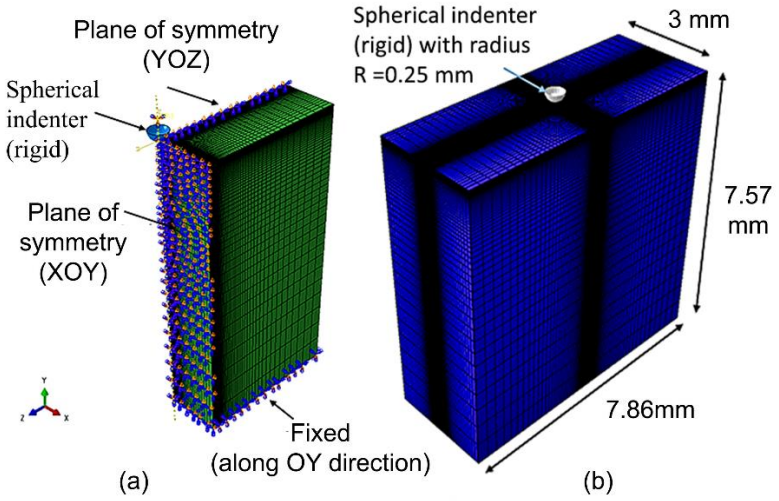

Figure 5: 3D mesh (3D th3-h7) with thickness of 3 mm (a) complete mesh with BC and (b) dimensions of the model

For each mesh, a simulation was run using the same BC, resulting in a load-displacement curve for each simulation. A comparison was made between the 3D model that represents the thin wall and the model

representing the larger specimen, where mechanical properties had not been affected by its dimensions. Considering the loading part of the F(h) curve, it has been noticed almost the same maximum load for both thin and large models for the same maximum penetration depth. So, neither the hardness nor the evolution of the loading part of the F(h) curve could be affected by the small thickness of the tested specimen.

The unloading part was then analysed to extract the Young's modulus from eq.3 (BASh equation) or eq.5 (BASh, Hay & Wolff equation) for each mesh used as shown in table 1. For mesh s984, the estimated error between the theoretical reduced modulus E_R (Theory) and the reduced modulus calculated from the indentation curve is equal to about 12.6% for BASh equation and 4.8% for BASh, Hay & Wolff equation This means that the correction made by Hay & Wolff is a better match for large scale models. For the 3D model (mesh 3D Ep30H7), a different result was obtained. Thus, the BASh equation without adopting the correction of Hay & Wolff leads to a minimum percentage of error for E_R (2.1%) while the corrected equation underestimates E_R (lowest value with a negative error of -5.4%).

	Theory	Mesh t984 f0.1		Mesh 3D Ep3-H7 f0.1	
		BASh	BASh-Hay & Wolff	BASh	BASh-Hay & Wolff
E_R (MPa)	127707	143813	133862	130391	120861
Error %		12.6	4.8	2.1	-5.4

Table 1: Values of E_R and percentage of error relative to the theory, using numerical simulation for indentation tests

The results show that despite the small width of the 3D indented sample, the value of the reduced modulus obtained from the indentation curve is quite close to the theoretical value. However, compared to an infinite half-space, the stiffness of the studied thin wall is slightly reduced due to the proximity of the radial free surface. The results therefore show that it is preferable to use the BASh method without the correction factor proposed by Hay and Wolff in order to obtain the least possible error when calculating the reduced modulus of elasticity of the thin wall obtained by AM.

4.2 Comparison between tensile and instrumented indentation test results

Tensile tests were performed on four different tensile specimens (Ti-5Nb, Ti-10Nb, Ti-40Nb and Ti-70Nb). On each shoulder of these specimens, indentation tests were performed using a spherical indenter. For each specimen, between 3 and 5 tensile and indentation tests were carried out. Fig.6 shows the experimental F(h) curves obtained by IIT and the stress-strain curves obtained via the tensile test.

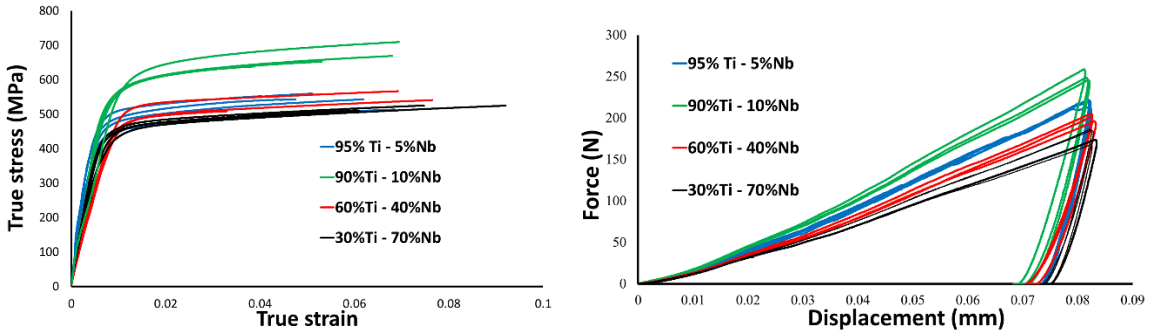

(a) (b)

Figure 6: a) True stress-strain curves obtained from tensile tests; b) Indentation curves

This figure shows that the evolution of the indentation curves is consistent with that of the tensile curves. The penetration resistance as well as the tensile strength are the highest for the Ti-10Nb specimen. The penetration resistance and the tensile strength are the lowest for the Ti-70Nb sample. The tensile and indentation tests also show significant heterogeneity in the different test specimens. Table 2 gives the values of the mechanical properties determined via IIT and tensile tests.

	95% Ti 5%Nb	90% Ti 10% Nb	60% Ti 40% Nb	30% Ti 70% Nb
	Instrumented Indentation Test			
E (GPa)	107±0.2	92±12	73±0.1	91±0.3
Re (MPa)	566±106	682±84	472±122	384±5
Rm (MPa)	646±22	753±33	600±6	498±34
n	0.070±0.064	0.074±0.032	0.118±0.082	0.113±0.016
σ for 6% strain (MPa)	668±12	795±38	612±28	519±29
Hardness obtained from the imprint (MPa)	2441±47	2686±71	2237±148	1944±83
	Tensile test			
E (GPa)	100±12	77±10	58±8	70±7
$Rp_{0,2}$ (MPa)	458±28	551±20	475±20	426±17
Rm (MPa)	510±23	630±22	513±19	480±4
σ for 6% strain (MPa)	538±21	664±27	533±27	509±5

Table 2: Mechanical properties determined via tensile test and via instrumented indentation techniques for each tensile specimen.

4.2.1 Comparison of Young's modulus depending on the characterization method.

The Young's modulus has been compared using both instrumented indentation and tensile tests. As previously indicated, the results of the instrumented indentation test, that has been undertaken on the shoulders of the tensile

specimen, are to be compared with the results of the tensile tests with the same chemical composition. In the case of IIT, since the shoulder size is very large in comparison to the size of the volume deformed by the indentation, the Young's modulus was calculated using eq.5.

The Young's modulus values obtained from the two methods are given in table 2 and compared in fig.7. Fig. 7 shows that the use of instrumented indentation leads to higher values for Young's modulus than those obtained from the tensile tests. Despite this, the Young's Modulus varies similarly with the two characterization methods. The Young's Modulus decreases for a niobium amount between 5% and 40%, and then increases until 70% of Nb.

Using X-ray diffraction patterns, the phases present in similar additively manufactured Ti-xNb alloys were identified in a previous paper for various chemical compositions [34]. It was shown that the Ti deposition consisted of a hexagonal α'-phase formed by the rapid cooling of columnar beta grains, and that when Nb content is ramped up to 25%, the high-temperature bcc β-phase was entirely retained. Fig.7 shows that Young's modulus for Ti-Nb alloys after SLM manufacturing and rapid cooling is dependent on the chemical composition. The addition of 5 and 10 wt% of Nb results in a decrease in Young's modulus. The first minimum in Young's modulus appears to be associated with the stability of the β phase. It is known that the β phase at high temperatures is retained by rapid cooling at a niobium content higher than 39 wt.% [36]–[38]. The values for the rapid cooling of Ti-Nb alloys in this work are in good agreement with those in the works of Ozaki et al. and Fedotov and Belousov [39], [40]. The second minimum in Young's modulus is observed for a composition of about 40% Nb.

Raabe et al.[41] have reported directional Young's modulus for binary Ti alloys (Ti-Nb and Ti-Mo) up to 40 wt.% with a composition variation of 11.5 wt.%. Ikehata et al.[42] have reported polycrystalline Young's modulus of binary Ti1- xMx (M = V, Nb, Mo, and W) alloys for x = 0.0, 0.25, 0.5, 0.75 and 1 with a specific structural configuration. The drop in Young's modulus between 0 and 20 wt. % has been widely studied in the literature. It was explained by the gradual increase in the rate of α" in martensite α' [40], [43]. The minimum is reached when the composition is 100 wt.% α". Young's modulus then increases due to a α" + β mixture and then decreases when the beta phase becomes preponderant [44]. A second minimum is reached when there is no more α". Finally, a soft increase in Young's modulus takes place from 40 wt.% because of the increase in stability of the β phase. The stability of the bcc β phase in the Ti-M alloys (M = transition element) can also be understood from the ratio of valence electrons and the number of atoms (e/a) reported in Fig.7 from Bönish et al [43]. It has been shown that the β phase in the Ti-Mo alloys is stabilized if the e/a ratio is equal to 4.2 or more [45]. In the Ti-Nb alloy system, the ratio e/a is superior or equal to 4.2, starting from Ti-22Nb. Thus, the minimum niobium content of ~36-39 wt.% is expected to stabilize the Ti-Nb β phase. The β phase stability of Ti-Nb system with 39 wt.% Nb content can also be understood using the bond order (Bo) and the d-orbital energy levels (Md), as discussed in reference [46]. As it can be seen, the β phase starts to become stable for a niobium content of more than 39 wt.%. The stability of the β phase can also correlate with the shear modulus $C' = (C11 - C12) / 2$ which is a {110} <110>.

However, addictive manufacturing, contrary to continuous casting, entails a very high cooling rate and a high oxygen content, which decrease the transformation temperature Ms in β titanium drastically [47], [48].

A previous study on the same FGM showed the exclusive presence of β phase from 25 wt.% [34], hence implying that the Gaussian curve observed by Fedotov (between 20 and 40 of Nb wt. %) may not exist in the case of additive manufacturing.

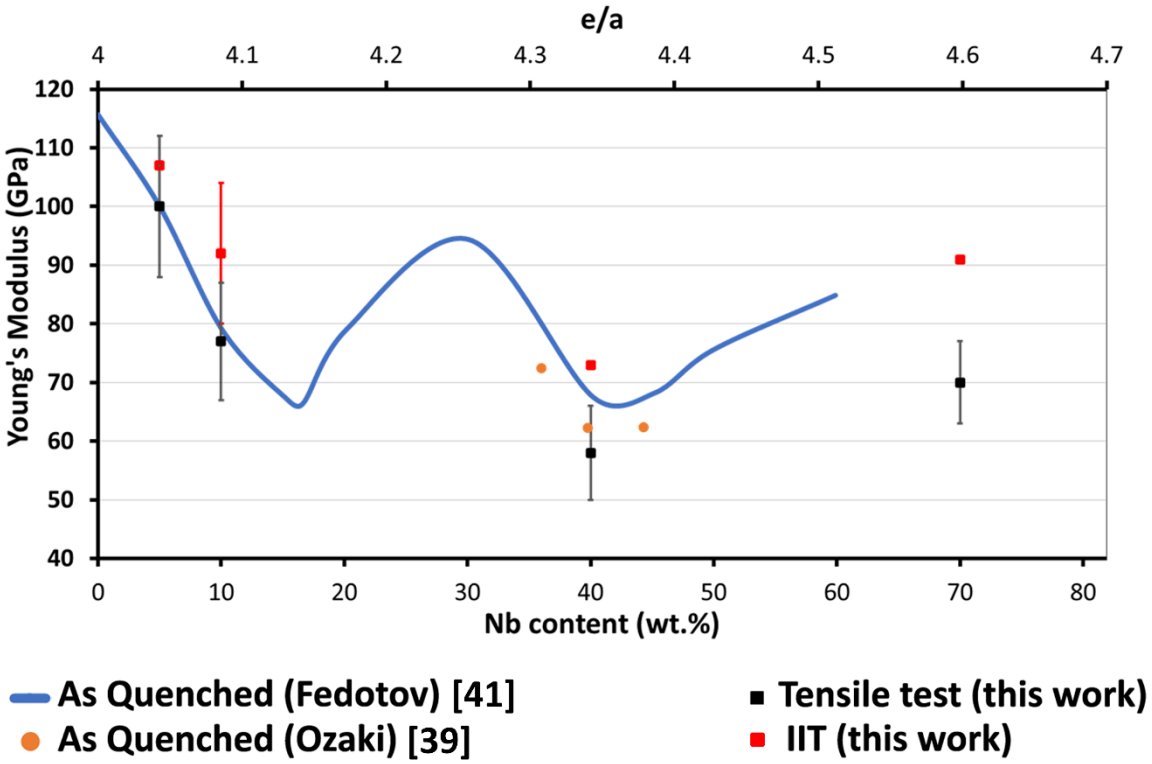

Figure 7: Nb content dependence of Young's modulus of Ti-xNb and e/a

4.2.2 Comparison of the work-hardening law depending on the characterization method

As for the Young's modulus, the stress-strain relationship of the instrumented indentation and that of the tensile test in the plastic regime have been compared.

Some authors have already proven the correlation between hardness and tensile strength [49], [50], and this is further proven in Table 2. In fact, the hardness depends on the yield strength as well as on the work-hardening exponent. A high yield strength and a high work-hardening exponent lead to a harder material whereas a low yield strength and a low work-hardening exponent lead to a material with a low hardness. Tabor et al. and Hernot et al. have shown the correlation between Vicker's hardness and tensile stress calculated for strain at 8%, for work-hardening materials [49], [50]. Various works have demonstrated that the spherical indentation curves are very similar for materials which present identical values of stress for the same representative strain in the range of 0.01-0.07, depending on the *h/R* values [13], [17], [19]. For the maximum value of the h/R ratio used in this study, the representative deformation is around 6%. That is the reason why fig.8 represents the evolution of the stress corresponding to a deformation of 6% as a function of the niobium amount.

Fig.8 shows that both tensile and indentation tests lead to the same evolution in the strength profile in function of the niobium percentage. The mechanical resistance increases when 5% and 10% of niobium is present and then

decreases progressively to reach its lowest value when there is 70% of niobium. Similarly, it can be observed from fig.8 that the stress for 6% strain obtained by the use of instrumented indentation is higher than that obtained by tensile tests.

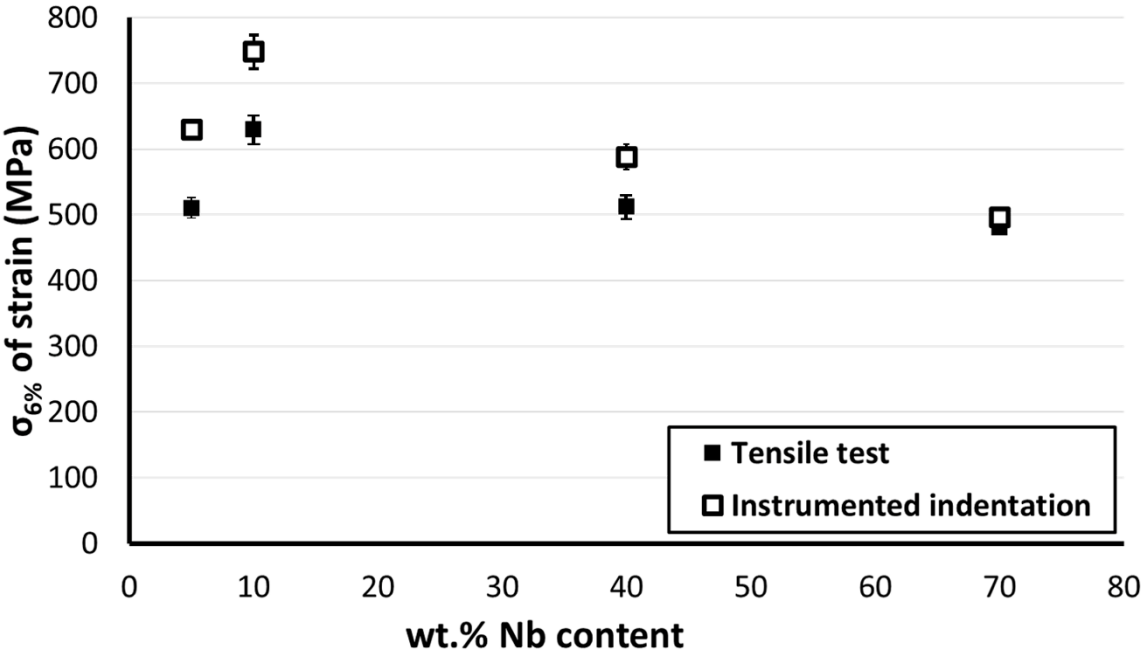

Figure 8: Comparison of the stress for 6% strain obtained by tensile tests and instrumented indentation for Ti-Nb alloy

From the representative stress-strain values obtained for various h/R ratios taken into account in this study, the Hollomon's hardening law given in eq.1 is obtained by an optimisation procedure. Fig.9 compares the results obtained from indentation and tensile tests. This figure shows the average work-hardening law obtained from indentation tests and the confidence interval which takes into account the material's heterogeneity and the experimental imprecisions.

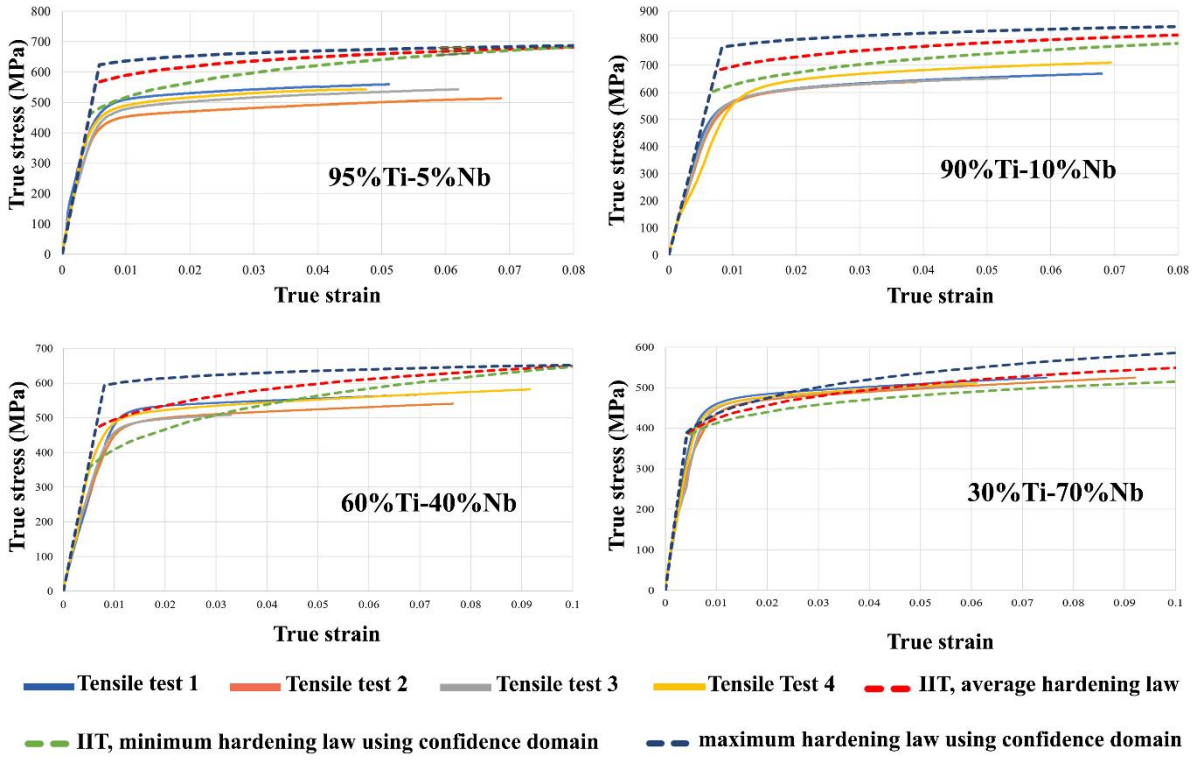

Figure 9: Comparison between hardening law identified by instrumented indentation and uniaxial tensile tests for Ti-Nb alloy

Due to the significant heterogeneity of the material, proven by a non-perfect reproducibility in the case of indentation and tensile tests (see Fig. 8), the confidence interval is relatively large. With the exception of the alloy containing 70% Nb, the indentation tests lead to the determination of the values of the work-hardening laws higher than those obtained by tensile tests. The difference in the studied alloys' behaviour between the tensile and the indentation test can be explained by the mechanical heterogeneity of the material. Indeed, if the surface strength of the tensile specimens is greater than that of the specimen's core, hardness tests performed on the surface lead to the characterization of a resistance higher than the one obtained from tensile tests. In order to check a possible mechanical heterogeneity between the surface and the section of the tensile specimen, micro-hardness tests were carried out on the 95%Ti-5%Nb alloy. This alloy was chosen because it presents the greatest difference between the hardening laws obtained by indentation and those obtained by tensile tests (fig.9). Micro and macro Vickers hardness tests were carried out on the surface of both longitudinal and cross-sectional areas of the tensile samples. The results, presented in fig.10, show that the hardness of the surface (i.e. where the instrumented indentation tests were performed) is slightly higher than that obtained in the core of the tensile specimen. The higher strength of the surface is more pronounced when using a 500 g load. This result indicates that the increase in strength in the section occurs in a thin surface layer of the tensile specimens. The increase in surface strength may therefore partly explain the difference between tensile and instrumented indentation test results. Since this increase is small over a relatively small surface layer, it may not be the only reason.

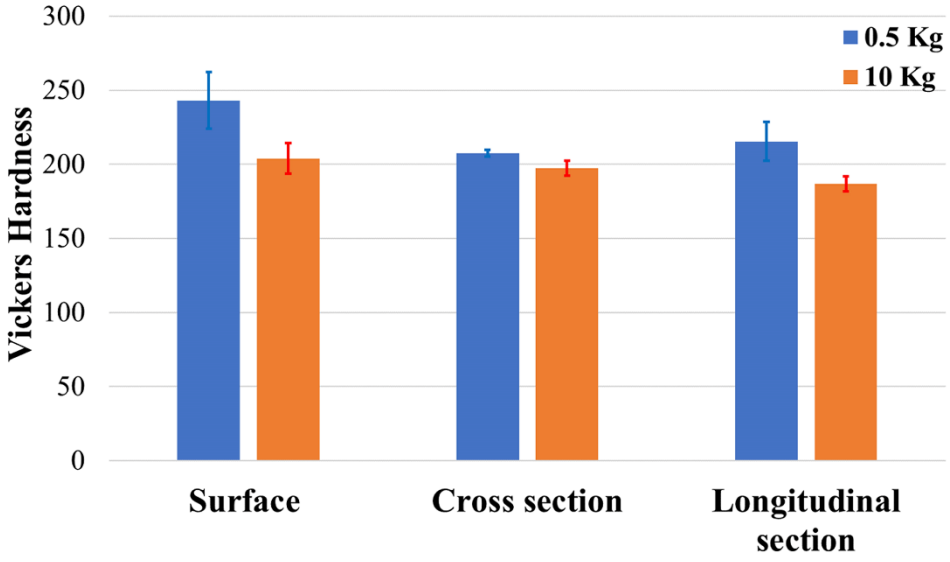

Figure 10: Micro and macro hardness obtained on the surface and in sections parallel and perpendicular to the tensile direction. Results for loads of 0.5 kg and 10 kg.

One explanation could be the great difference in volumes mechanically characterized by tensile and indentation tests. A recent study on Ti64 alloys obtained by PBF-SLM process shows that the work-hardening law obtained from a tensile test depends on the volume of the sample [51] . The authors explain that this influence is due to the difference in surface/volume ratios, thermal history and the number of defects in the samples.

During the building of the FGM wall and of the tensile test specimens using the DED-CLAD® process, layer height step was set in the range of 0.5 to 0.8 mm. The microstructural study carried out in the paper by Maunoury et al. [34] showed that additively manufactured grains could have different sizes and shapes for the same layer. Tomographic tests have shown that no more than 1% of the unmelted particles are present in the deposited material. Analysis by optical microscopy have also shown that the percentage of the unmelted particles was inferior to 4%. However, these results revealed that the few unmelted Nb particles were heterogeneously distributed and appeared to be localized at the interfaces between two deposited tracks. Tensile tests on Ti-Nb specimens of different dimensions could be carried out in order to examine the influence of the volume size on the identified work-hardening law.

The difference in results obtained using both tensile and indentation tests could also be due to the anisotropy behaviour law of Ti-Nb alloy. Uniaxial tensile test results in the introduction of pure tensile stress or tensile-shear stress, depending on the orientation of the section. An indentation test results in the introduction of compressive, tensile, and shear stresses depending on the orientation and location of the plane in the indented material. The field of compressive plastic deformation is the most extensive and the highest in intensity. A recent study on Ti64 alloys made by laser powder bed fusion (L-PBF) shows a difference in results depending on whether the applied stresses are in shear or in tension [52]. On these same alloys, an applied load in the directions parallel and perpendicular to the build direction also leads to different strain-hardening laws [52]. This difference could be caused by a specific orientation of the additive manufactured grains. In ref. [34], the crystallographic examination carried out on the studied Ti-xNb alloys showed that the grains tend to be elongated along the building direction of the wall. The anisotropic character of the constitutive equation of pure

titanium α-Ti and titanium alloy Ti64 was also determined respectively by Benmhenni et al. [53] and Tuninetti et al. [54]. The results obtained on pure titanium α-Ti and titanium alloy Ti64 show that the compressive strength of these materials is higher than the tensile strength. In order to understand the differences observed between tensile and indentation test results, tensile and compressive tests will have to be carried out in different directions in order to verify the isotropic or anisotropic character of the Ti-Nb alloys studied in this work.

5. Characterization of the Ti-xNb FGM material using only IIT

Results obtained from both spherical indentation and tensile tests revealed the similar evolution for mechanical properties regardless of the percentage of the presented niobium. The slightly higher values for Young's modulus obtained by IIT relative to the tensile test, and good correlation of the hardening law at 6% of deformation, validate the use of the instrumented indentation test as a means of identifying the mechanical properties of the FGM Ti-xNb alloy.

5.1 F(h) curves of Ti-xNb alloy

Six indentation tests were performed on the Ti6Al4V substrate, as shown in fig.11a. The corresponding F(h) curves reveal a similar evolution during the loading phase for five indentations, however, test n°5 presents a F(h) curve located above the others. This result is explained by a higher penetration resistance, which is consistent with the position of the indentation (near the heat-affected layer, see fig.3). This increase in hardness is due to the microstructure modification from α+β to α' [34] .

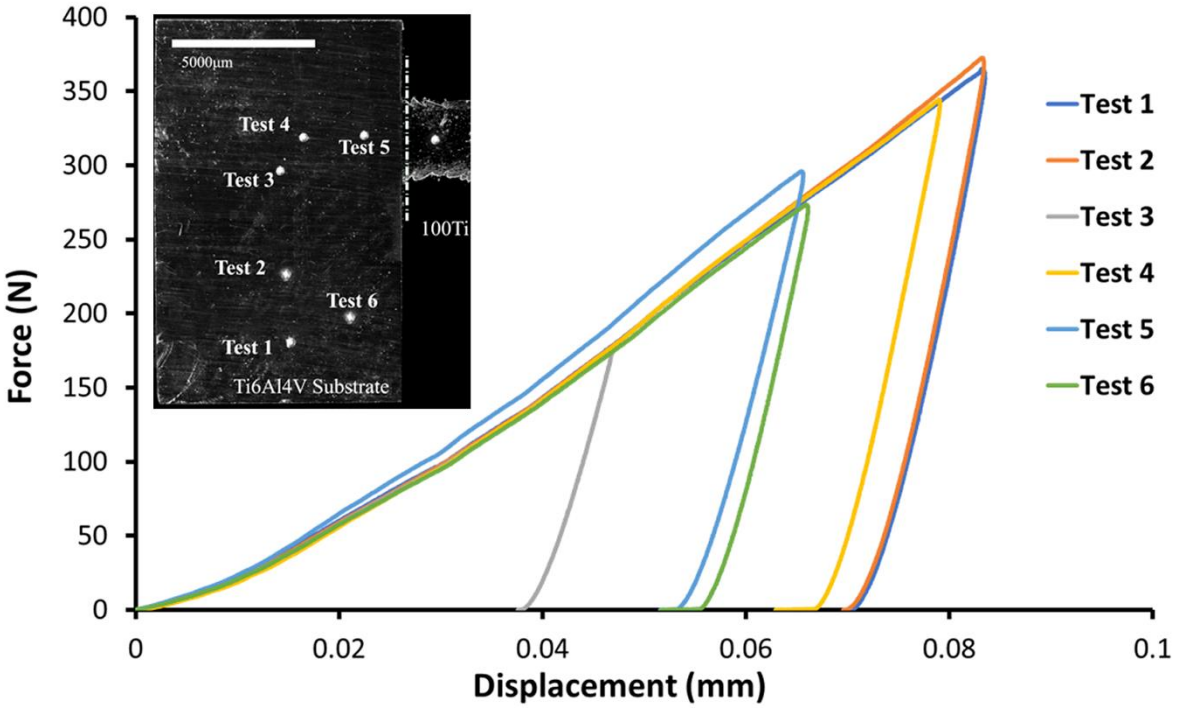

(a)

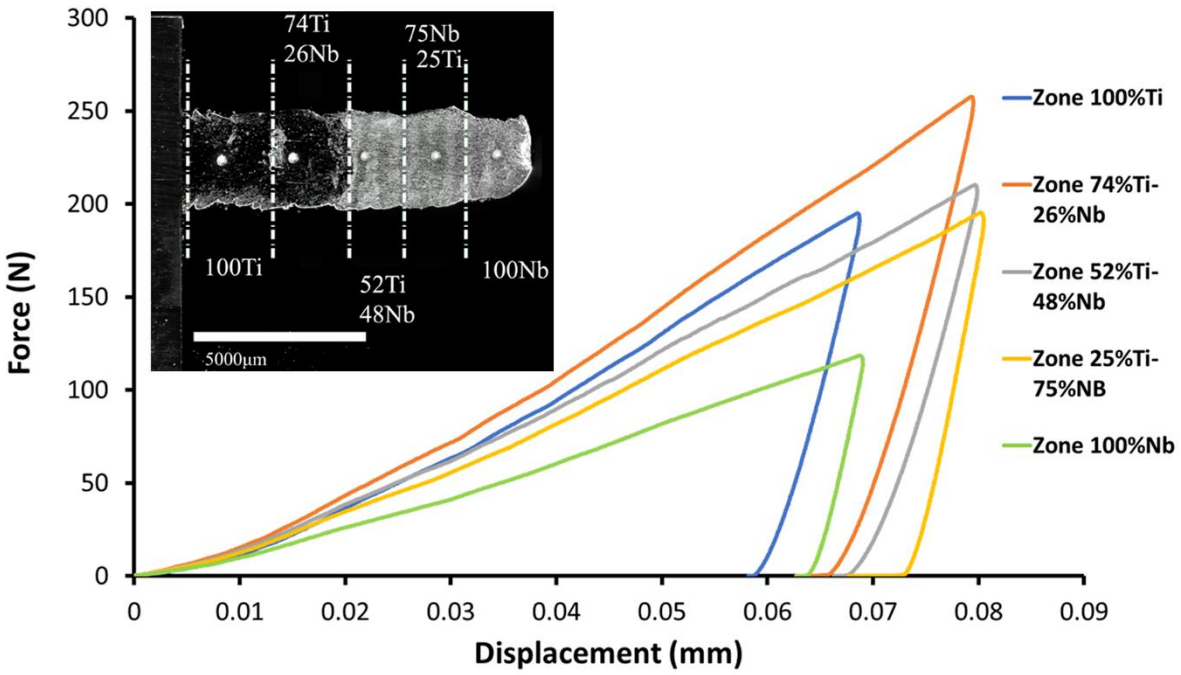

(b)

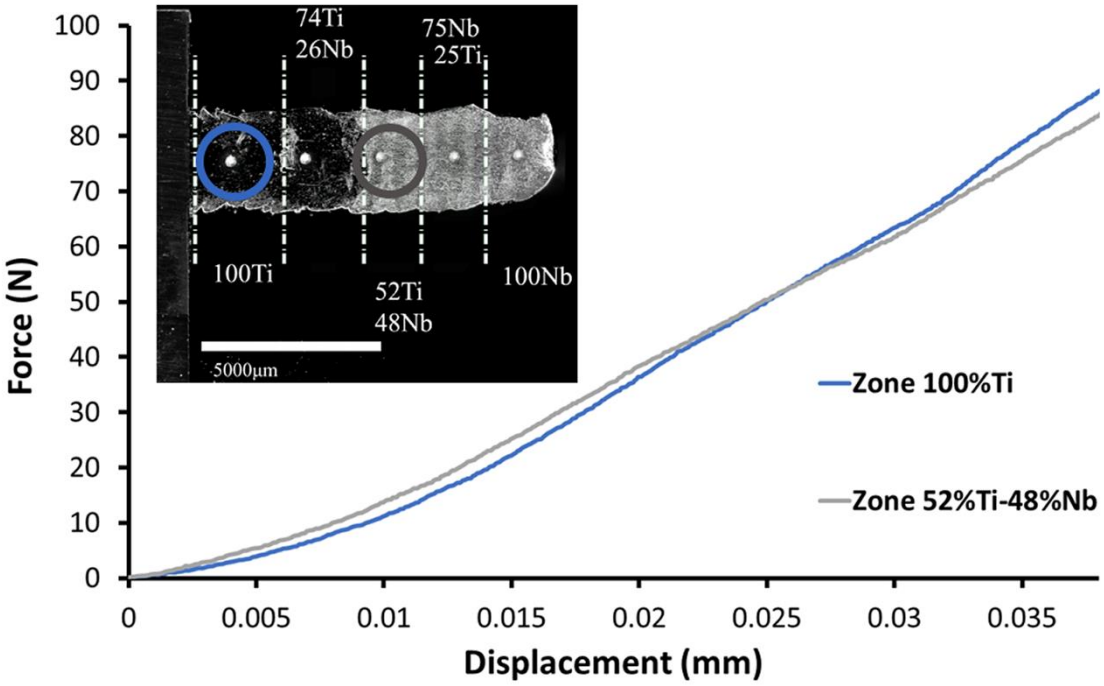

(c)

Figure 11: F(h) curves obtained (a) on the Ti6Al4V substrate, (b) for each gradient of the Ti-Nb wall and (c) focus on 100% Ti and 52%Ti-48%Nb

Indentation tests were then performed on each chemical layer of the FGM part. Fig.11b reveals that the more the niobium is present, the less the penetration resistance is important, except for the materials composed of very low percentage of niobium (smaller than 26% Nb). The pure titanium metal presents a difference of behaviour compared to the Ti-xNb material composed by 48% Nb. In fact, for a penetration inferior to 0.025 mm, the pure

titanium alloy tends to be of lesser resistance than that of 48% Nb. Beyond 0.025 mm, the trend is reversed. This result indicates that for high penetration values, the pure titanium alloy is harder than the alloy with 48% Nb (fig.11c). Assuming that both alloys (100%Ti and 52%Ti-48%Nb) are homogeneous, the first metal seems to have a higher strain hardening exponent [55].

5.2 Hardness of the FGM Ti-xNb alloy

From the measured imprints and the maximal load, hardness has been determined on the substrate and for each gradient of composition. The substrate has a similar hardness in different locations except in the heat-affected zone where the value is higher (around 3890 MPa and 4182 MPa, respectively). This result confirms the previous observation on F(h) curves.

The wall presents a variation of hardness depending on the chemical composition of each zone, as shown in fig.12. Pure Titanium has a hardness of 2700 MPa which is much lower than the hardness of the Ti6Al4V substrate (around of 4000 MPa). When the niobium content is in the range of 0-25%, the hardness increases to 3000 MPa which is consistent with the Vickers microhardness [34] . This increase in the hardness was explained by some authors by the presence of a small fraction of ω-phase [44], [56]. When the niobium content increased further, the microhardness gradually decreased which is also consistent with the Vickers microhardness [34].

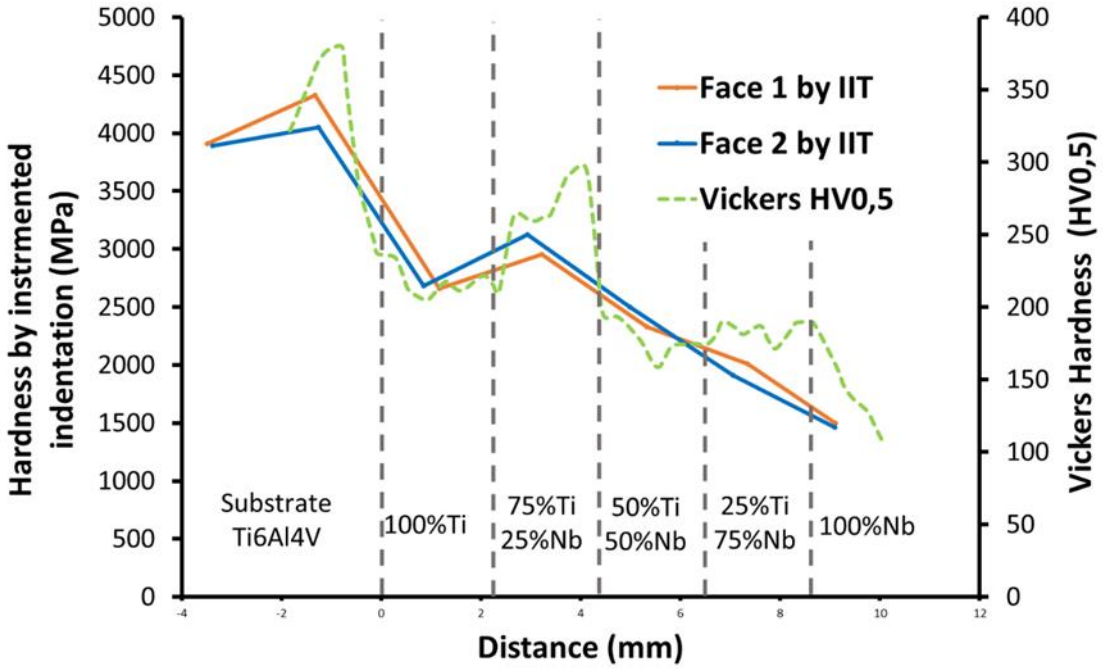

Figure 12: Evolution of the hardness using instrumented indentation on the Ti-Nb wall. Measurement on the two faces of the wall and average of the results.

5.3 Mechanical properties of Ti-xNb alloy obtained by instrumented indentation

The values of the yield strength, the stress for 6% strain, the tensile strength, Young's modulus and the work-hardening exponent obtained by the Moussa et al. method are given in Table 3. It can be seen that the yield

strength, the stress for 6% strain and the tensile strength obtained from F(h) curves follow the same evolution, function of % Nb, as that of the hardness obtained from the imprints. It is also confirmed from Table 3 that the work-hardening exponent of the pure Ti metal (100% Ti) is the highest in the wall part of the Ti-xNb specimen. By comparing the results obtained on the tensile samples and on the FGM thin wall, it is noticed that both tensile and indentation tests lead to the same evolution in the strength profile in function of the niobium percentage (see tables 2 and 3). The mechanical resistance increases for a niobium amount between 5% and 26 wt%, and then decreases until 100% of Nb.

The reduced modulus of contact, E_R, was calculated from the indentation curve using eq.3. From E_R, Young's modulus of the indented material can be calculated using the Poisson coefficient of the indented material and the elastic properties of the indenter (eq.4). The elastic properties of the indenter are given in section 3.4, the Poisson ratio of pure Ti is fixed at 0.34 and that of pure niobium at 0.38 [57]. For Ti-Nb alloys, it was assumed that the value of the Poisson ratio follows the evolution of the percentage of niobium. Table 3 shows Young's modulus values obtained from ITT technique for the substrate and the various zones of the Ti-Nb thin wall. The addition of niobium between 0% and 48% leads to a decrease in Young's Modulus while a niobium amounts up to 100% leads to an increase of Young's Modulus. Similar results were obtained for tensile specimens (Table 2). Indeed, for a quantity of Nb lower than 40%, niobium addition leads to a decrease in Young's Modulus, whereas from this value and up to 70% of Nb, the addition of niobium leads to an increase in this parameter. Moreover, values obtained for some layers of the Ti-Nb thin wall are consistent with those found in the literature: E=102 GPa for Ti with DED process[58], E=78 GPa for 26% of Nb [59] and E=104 GPa for pure niobium [60].

	Ti6Al4V Substrate	100% Ti	74% Ti 26% Nb	52% Ti 48% Nb	25% Ti 75% Nb	100% Nb
Re (MPa)	950±50	476±125	751±30	677±149	464±51	224±13
Rm (MPa)	1196±66	800±127	917±45	738±24	571±13	427±18
E (GPa)	118±5	90±5	79±5	73±2	92±5	100±2
n	0.131±0.034	0.202±0.077	0.126±0.025	0.076±0.026	0.103±0.102	0.189±0.0002
σ for 6% strain (MPa)	-	722±22	855±5	687±7	563±5	395±15
Hardness obtained from the imprint (MPa)	3890±50	2674±8	3040±60	2415±58	1960±36	1482±12

Table 3: Mechanical properties obtained by instrumented indentation for each layer of the FGM

6. Conclusion

This paper first proposed the validation of the instrumented indentation method by comparing indentation and tensile test results performed on homogeneous Ti-xNb alloys (x=5, 10, 40 and 70 wt%) obtained by additive manufacturing. The mechanical properties vary similarly, in particular Young's Modulus and the stress

calculated for a 6% strain, regardless of the method used (instrumented indentation or tensile tests). Then, on the basis of this validation, the mechanical properties for each layer of a Ti-xNb FGM specimen (x=0, 26, 48, 75 and 100 wt%) obtained by additive manufacturing were identified. The main conclusions which can be outlined are:

- Each layer of the FGM was successfully tested using spherical indentation to get several mechanical properties such as Young's modulus, hardness, yield stress, tensile strength and work-hardening exponent regardless of their small dimensions.
- Results of indentation tests performed on FGM specimens and on homogeneous tensile specimens show that the evolution of the mechanical properties as a function of niobium amount is complex. This evolution seems to depend particularly on the stability of the β phase and the presence of a fraction of the ω-phase. For all the compositions of the Ti-Nb FGM, Young's Modulus values obtained from instrumented indentation are consistent with results found in the literature. Moreover, the study on FGM shows that up to 26% of niobium, adding niobium leads to an increase in strength, while further addition of niobium results in a decrease in strength.

Additive manufacturing provides FGMs easily, quickly and in small volumes, avoiding the specific production of cast alloys for each composition. Furthermore, instrumented indentation enables the mechanical characterisation for small volumes of material. This paper demonstrates the interest of coupling the additive manufacturing technique with the instrumented indentation method for a rapid characterisation of a wide range of alloys, the use of both techniques being useful for the optimized design of additively manufactured FGMS.

Acknowledgments

The authors acknowledge H.C. Starck Tantalum and Niobium GmbH, powder manufacturer, for providing the pre-alloyed Ti44Nb powder; Patrick MOLL for his assistance during the tensile tests.

References

[1] Clément Margueray and Loïc Vollard, "Fabrication additive métallique : technologies et opportunités," *INSA Rouen*, p. 36, 2015.
[2] ASTM International, *Standard terminology for additive manufacturing technologies*. West Conshohocken, PA : ASTM International, 2012.
[3] E. Chlebus, B. Kuźnicka, R. Dziedzic, and T. Kurzynowski, "Titanium alloyed with rhenium by selective laser melting," *Mater. Sci. Eng. A*, vol. 620, pp. 155–163, Jan. 2015, doi: 10.1016/j.msea.2014.10.021.
[4] P. C. Collins, R. Banerjee, S. Banerjee, and H. L. Fraser, "Laser deposition of compositionally graded titanium–vanadium and titanium–molybdenum alloys," *Mater. Sci. Eng. A*, vol. 352, no. 1–2, pp. 118–128, Jul. 2003, doi: 10.1016/S0921-5093(02)00909-7.
[5] B. E. Carroll *et al.*, "Functionally graded material of 304L stainless steel and inconel 625 fabricated by directed energy deposition: Characterization and thermodynamic modeling," *Acta Mater.*, vol. 108, pp. 46–54, Apr. 2016, doi: 10.1016/j.actamat.2016.02.019.
[6] W. Z. Bakar, S. Basri, S. N. Jamaludin, and A. Sajjad, "Functionally Graded Materials: An Overview of Dental Applications," *World J. Dent.*, p. 8.
[7] V. Birman, "Functionally Graded Materials and Structures," in *Encyclopedia of Thermal Stresses*, R. B. Hetnarski, Ed. Dordrecht: Springer Netherlands, 2014, pp. 1858–1865.

[8] S. Heuer *et al.*, "Ultra-fast sintered functionally graded Fe/W composites for the first wall of future fusion reactors," *Compos. Part B Eng.*, vol. 164, pp. 205–214, May 2019, doi: 10.1016/j.compositesb.2018.11.078.
[9] A. Sola, D. Bellucci, and V. Cannillo, "Functionally graded materials for orthopedic applications – an update on design and manufacturing," *Biotechnol. Adv.*, vol. 34, no. 5, pp. 504–531, Sep. 2016, doi: 10.1016/j.biotechadv.2015.12.013.
[10] H. H. Zhang, S. Y. Han, L. F. Fan, and D. Huang, "The numerical manifold method for 2D transient heat conduction problems in functionally graded materials," *Eng. Anal. Bound. Elem.*, vol. 88, pp. 145–155, Mar. 2018, doi: 10.1016/j.enganabound.2018.01.003.
[11] W. Zhen, M. Yuting, R. Xiaohui, and S. H. Lo, "Analysis of Functionally Graded Plates Subjected to Hygrothermomechanical Loads," *AIAA J.*, vol. 54, no. 11, pp. 3667–3673, 2016, doi: 10.2514/1.J054714.
[12] D. C. Hofmann *et al.*, "Developing gradient metal alloys through radial deposition additive manufacturing," *Sci. Rep.*, vol. 4, p. 5357, Jun. 2014, doi: 10.1038/srep05357.
[13] Y. P. Cao and J. Lu, "A new method to extract the plastic properties of metal materials from an instrumented spherical indentation loading curve," *Acta Mater.*, vol. 52, no. 13, pp. 4023–4032, Aug. 2004, doi: 10.1016/j.actamat.2004.05.018.
[14] M. Dao, N. Chollacoop, K. J. Van Vliet, T. A. Venkatesh, and S. Suresh, "Computational modeling of the forward and reverse problems in instrumented sharp indentation," *Acta Mater.*, vol. 49, no. 19, pp. 3899–3918, Nov. 2001, doi: 10.1016/S1359-6454(01)00295-6.
[15] J. H. Lee, D. Lim, H. Hyun, and H. Lee, "A numerical approach to indentation technique to evaluate material properties of film-on-substrate systems," *Int. J. Solids Struct.*, vol. 53, no. 9, 2005, doi: 10.1016/j.ijsolstr.2012.01.001.
[16] L. Meng, B. Raghavan, O. Bartier, X. Hernot, G. Mauvoisin, and P. Breitkopf, "An objective meta-modeling approach for indentation-based material characterization," *Mech. Mater.*, vol. 107, pp. 31–44, Apr. 2017, doi: 10.1016/j.mechmat.2017.01.011.
[17] C. Moussa, X. Hernot, O. Bartier, G. Delattre, and G. Mauvoisin, "Identification of the hardening law of materials with spherical indentation using the average representative strain for several penetration depths," *Mater. Sci. Eng. A*, vol. 606, pp. 409–416, Jun. 2014, doi: 10.1016/j.msea.2014.03.123.
[18] W. C. Oliver and G. M. Pharr, "An improved technique for determining hardness and elastic modulus using load and displacement sensing indentation experiments," *J. Mater. Res.*, vol. 7, no. 6, pp. 1564–1583, Jun. 1992, doi: 10.1557/JMR.1992.1564.
[19] M. Zhao, N. Ogasawara, N. Chiba, and X. Chen, "A new approach to measure the elastic–plastic properties of bulk materials using spherical indentation," *Acta Mater.*, vol. 54, no. 1, pp. 23–32, Jan. 2006, doi: 10.1016/j.actamat.2005.08.020.
[20] N. A. Branch, G. Subhash, N. K. Arakere, and M. A. Klecka, "A new reverse analysis to determine the constitutive response of plastically graded case hardened bearing steels," *Int. J. Solids Struct.*, vol. 48, no. 3, pp. 584–591, Feb. 2011, doi: 10.1016/j.ijsolstr.2010.10.023.
[21] M. Idriss, O. Bartier, G. Mauvoisin, and X. Hernot, "Determining the stress level of monotonic plastically pre-hardened metal sheets using the spherical instrumented indentation technique," *J. Mech. Sci. Technol.*, vol. 33, no. 1, pp. 183–195, Jan. 2019, doi: 10.1007/s12206-018-1218-1.
[22] J. J. Kim, T.-H. Pham, and S.-E. Kim, "Instrumented indentation testing and FE analysis for investigation of mechanical properties in structural steel weld zone," *Int. J. Mech. Sci.*, vol. 103, pp. 265–274, Nov. 2015, doi: 10.1016/j.ijmecsci.2015.09.015.
[23] J. H. Lee, T. Kim, and H. Lee, "A study on robust indentation techniques to evaluate elastic–plastic properties of metals," *Int. J. Solids Struct.*, vol. 47, no. 5, pp. 647–664, Mar. 2010, doi: 10.1016/j.ijsolstr.2009.11.003.
[24] C. Moussa, O. Bartier, X. Hernot, G. Mauvoisin, J.-M. Collin, and G. Delattre, "Mechanical characterization of carbonitrided steel with spherical indentation using the average representative strain," *Mater. Des.*, vol. 89, pp. 1191–1198, Jan. 2016, doi: 10.1016/j.matdes.2015.10.067.
[25] S. Nagaraju, J. GaneshKumar, P. Vasantharaja, M. Vasudevan, and K. Laha, "Evaluation of strength property variations across 9Cr-1Mo steel weld joints using automated ball indentation (ABI) technique," *Mater. Sci. Eng. A*, vol. 695, pp. 199–210, May 2017, doi: 10.1016/j.msea.2017.04.021.
[26] L. Sow, S. Kamali-Bernard, O. Bartier, G. Mauvoisin, and F. Bernard, "Experimental Estimation of the Elastic Modulus of Non-Hazardous Waste Incineration Bottom Ash Aggregates by Indentation Tests - Microanalysis of Particles by Scanning Electron Microscopy," *Advanced Materials Research*, 2018. /amr.1145.80 (accessed Mar. 09, 2020).
[27] M. Zhao, X. Han, G. Wang, and G. Xu, "Determination of the mechanical properties of surface-modified layer of 18CrNiMo7-6 steel alloys after carburizing heat treatment," *Int. J. Mech. Sci.*, vol. 148, pp. 84–93, Nov. 2018, doi: 10.1016/j.ijmecsci.2018.08.021.

[28] C. Schneider-Maunoury, L. Weiss, P. Acquier, D. Boisselier, and P. Laheurte, “Functionally graded Ti6Al4V-Mo alloy manufactured with DED-CLAD® process,” *Addit. Manuf.*, vol. 17, pp. 55–66, Oct. 2017, doi: 10.1016/j.addma.2017.07.008.
[29] O’Neil, *Hardness Measurements of Metals and Alloys*. Oxford: Clarendon, 1951.
[30] S. I. Bulychev, V. P. Alekhin, M. K. Shorshorov, A. P. Ternovskii, and G. D. Shnyrev, “Determining Young’s modulus from the indentor penetration diagram,” *Ind Lab USSR*, vol. 41, pp. 1409–1412, Sep. 1975.
[31] S. I. Bulychev, V. P. Alekhin, M. K. Shorshorov, and A. P. Ternovskii, “Mechanical properties of materials studied from kinetic diagrams of load versus depth of impression during microimpression,” *Strength Mater.*, vol. 8, no. 9, pp. 1084–1089, Sep. 1976, doi: 10.1007/BF01529860.
[32] J. L. Hay and P. J. Wolff, “Small correction required when applying the Hertzian contact model to instrumented indentation data,” *J. Mater. Res.*, vol. 16, no. 5, pp. 1280–1286, May 2001, doi: 10.1557/JMR.2001.0179.
[33] J. L. Murray, “The Nb−Ti (Niobium-Titanium) system,” *Bull. Alloy Phase Diagr.*, vol. 2, no. 1, pp. 55–61, Jun. 1981, doi: 10.1007/BF02873704.
[34] C. Schneider-Maunoury, L. Weiss, O. Perroud, D. Joguet, D. Boisselier, and P. Laheurte, “An application of differential injection to fabricate functionally graded Ti-Nb alloys using DED-CLAD® process,” *J. Mater. Process. Technol.*, vol. 268, pp. 171–180, Jun. 2019, doi: 10.1016/j.jmatprotec.2019.01.018.
[35] Y. Combres, “Propriétés du titane et de ses alliages,” p. 21, 2010.
[36] H. Y. Kim, S. Hashimoto, J. I. Kim, H. Hosoda, and S. Miyazaki, “Mechanical Properties and Shape Memory Behavior of Ti-Nb Alloys,” *Mater. Trans.*, vol. 45, no. 7, pp. 2443–2448, 2004, doi: 10.2320/matertrans.45.2443.
[37] H. Y. Kim, Y. Ikehara, J. I. Kim, H. Hosoda, and S. Miyazaki, “Martensitic transformation, shape memory effect and superelasticity of Ti–Nb binary alloys,” *Acta Mater.*, vol. 54, no. 9, pp. 2419–2429, May 2006, doi: 10.1016/j.actamat.2006.01.019.
[38] M. Tane, K. Hagihara, M. Ueda, T. Nakano, and Y. Okuda, “Elastic-modulus enhancement during room-temperature aging and its suppression in metastable Ti–Nb-Based alloys with low body-centered cubic phase stability,” *Acta Mater.*, vol. 102, pp. 373–384, Jan. 2016, doi: 10.1016/j.actamat.2015.09.030.
[39] T. Ozaki, H. Matsumoto, S. Watanabe, and S. Hanada, “Beta Ti Alloys with Low Young’s Modulus,” *Mater. Trans.*, vol. 45, no. 8, pp. 2776–2779, 2004, doi: 10.2320/matertrans.45.2776.
[40] Fedotov, S.G., Belousov, “Elastic constants of alloys of the system titanium niobium.,” *Phys. Met. Metallogr.*, vol. 17, pp. 83–86, 1964.
[41] D. Raabe, B. Sander, M. Friák, D. Ma, and J. Neugebauer, “Theory-guided bottom-up design of β-titanium alloys as biomaterials based on first principles calculations: Theory and experiments,” *Acta Mater.*, vol. 55, no. 13, pp. 4475–4487, Aug. 2007, doi: 10.1016/j.actamat.2007.04.024.
[42] H. Ikehata, N. Nagasako, T. Furuta, A. Fukumoto, K. Miwa, and T. Saito, “First-principles calculations for development of low elastic modulus Ti alloys,” *Phys. Rev. B*, vol. 70, no. 17, p. 174113, Nov. 2004, doi: 10.1103/PhysRevB.70.174113.
[43] M. Bönisch *et al.*, “Composition-dependent magnitude of atomic shuffles in Ti–Nb martensites,” *J. Appl. Crystallogr.*, vol. 47, no. 4, Art. no. 4, Aug. 2014, doi: 10.1107/S1600576714012576.
[44] C. M. Lee, C. P. Ju, and J. H. Chern Lin, “Structure-property relationship of cast Ti-Nb alloys,” *J. Oral Rehabil.*, vol. 29, no. 4, pp. 314–322, Apr. 2002, doi: 10.1046/j.1365-2842.2002.00825.x.
[45] A. V. Dobromyslov and V. A. Elkin, “Martensitic transformation and metastable ß-phase in binary titanium alloys with beta-metals of 4-6 periods,” *J. Phys. IV Proc.*, vol. 112, pp. 723–726, Oct. 2003, doi: 10.1051/jp4:2003984.
[46] M. Abdel-Hady, K. Hinoshita, and M. Morinaga, “General approach to phase stability and elastic properties of β-type Ti-alloys using electronic parameters,” *Scr. Mater.*, vol. 55, no. 5, pp. 477–480, Sep. 2006, doi: 10.1016/j.scriptamat.2006.04.022.
[47] J. I. Kim, H. Y. Kim, H. Hosoda, and S. Miyazaki, “Shape Memory Behavior of Ti--22Nb--(0.5--2.0)O(at%) Biomedical Alloys,” p. 6.
[48] E. G. Obbard *et al.*, “The effect of oxygen on α’’ martensite and superelasticity in Ti-24Nb-4Zr-8Sn,” *Acta Mater.*, vol. 59, no. 1, pp. 112–125, 2011, doi: 10.1016/j.actamat.2010.09.015.
[49] D. Tabor, *The Hardness of Metals*. OUP Oxford, 1951.
[50] X. Hernot, C. Moussa, and O. Bartier, “Study of the concept of representative strain and constraint factor introduced by Vickers indentation,” *Mech. Mater.*, vol. 68, pp. 1–14, Jan. 2014, doi: 10.1016/j.mechmat.2013.07.004.
[51] J. Dzugan *et al.*, “Effects of thickness and orientation on the small scale fracture behaviour of additively manufactured Ti-6Al-4V,” *Mater. Charact.*, vol. 143, pp. 94–109, Sep. 2018, doi: 10.1016/j.matchar.2018.04.003.

[52] T. DebRoy *et al.*, “Additive manufacturing of metallic components – Process, structure and properties,” *Prog. Mater. Sci.*, vol. 92, pp. 112–224, Mar. 2018, doi: 10.1016/j.pmatsci.2017.10.001.
[53] N. Benmhenni, S. Bouvier, R. Brenner, T. Chauveau, and B. Bacroix, “Micromechanical modelling of monotonic loading of CP α-Ti: Correlation between macroscopic and microscopic behaviour,” *Mater. Sci. Eng. A*, vol. 573, pp. 222–233, Jun. 2013, doi: 10.1016/j.msea.2013.02.022.
[54] V. Tuninetti, G. Gilles, O. Milis, T. Pardoen, and A. M. Habraken, “Anisotropy and tension–compression asymmetry modeling of the room temperature plastic response of Ti–6Al–4V,” *Int. J. Plast.*, vol. 67, pp. 53–68, Apr. 2015, doi: 10.1016/j.ijplas.2014.10.003.
[55] Taljat B., Zacharia T., Kosel F., “New analytical procedure to determine stress–strain curve from spherical indentation data,” *Int J Solids Struct*, vol. 33, no. 33, 1998.
[56] A. Thoemmes, I. A. Bataev, N. S. Belousova, and D. V. Lazurenko, “Microstructure and mechanical properties of binary Ti-Nb alloys for application in medicine,” in *2016 11th International Forum on Strategic Technology (IFOST)*, Novosibirsk, Russia, Jun. 2016, pp. 26–29, doi: 10.1109/IFOST.2016.7884101.
[57] “Titanium, Ti.” http://www.matweb.com/search/datasheet.aspx?bassnum=METi00&ckck=1 (accessed Mar. 09, 2020).
[58] H. Attar, M. J. Bermingham, S. Ehtemam-Haghighi, A. Dehghan-Manshadi, D. Kent, and M. S. Dargusch, “Evaluation of the mechanical and wear properties of titanium produced by three different additive manufacturing methods for biomedical application,” *Mater. Sci. Eng. A*, vol. 760, pp. 339–345, Jul. 2019, doi: 10.1016/j.msea.2019.06.024.
[59] Y.-H. Hon, J.-Y. Wang, and Y.-N. Pan, “Composition/Phase Structure and Properties of Titanium-Niobium Alloys,” *Mater. Trans.*, vol. 44, no. 11, pp. 2384–2390, 2003, doi: 10.2320/matertrans.44.2384.
[60] “Niobium | Plansee.” https://www.plansee.com/fr/materiaux/niobium.html (accessed Apr. 03, 2020).